OPEN ACCESS
JOURNAL OF ADVANCED DIELECTRICS
Vol. 12, No. 4 (2022) 2244003 (7 pages)

DOI: 10.1142/S2010135X22440039

# Performance enhancement of ultrasonic transducer made of textured PNN-PZT ceramic

Lang Bian[*,§,#], Ke Zhu[*,#], Qian Wang[*], Jinpeng Ma[*], Jinhui Fan[*], Xudong Qi[†], Guicheng Jiang[*], Bo Zhao[*], Rui Zhang[*], Bin Yang[*,‖] and Wenwu Cao[‡]

[*]*School of Instrumentation Science and Engineering, Harbin Institute of Technology Harbin 150080, P. R. China*

[†]*School of Physics and Electronic Engineering, Harbin Normal University Harbin 150025, P. R. China*

[‡]*Materials Research Institute, The Pennsylvania State University, University Park Pennsylvania 16802, USA*

[§]bianlang@hit.edu.cn

[‖]binyang@hit.edu.cn

Received 14 June 2022; Revised 22 July 2022; Accepted 3 August 2022; Published 20 August 2022

In this paper, $0.36Pb(Ni_{1/3}Nb_{2/3})O_3$–$0.24PbZrO_3$–$0.40PbTiO_3$(PNN-PZT) ceramic was prepared, and texture engineering was performed on this PNN-PZT ceramic to improve its electromechanical properties and temperature stability. Single element ultrasonic transducers were prepared using PNN-PZT, PNN-PZT textured ceramics, and their performance were evaluated and compared using a PZT-5H ceramic based transducer as the benchmark. It is shown that the sensitivity and bandwidth of the PNN-PZT textured ceramic-based transducer are much superior to regular PNN-PZT ceramic and PZT-5H ceramic based transducers.

*Keywords*: Textured ceramic; ultrasonic transducer; PNN-PZT.

## 1. Introduction

Single element ultrasound transducers are widely used in nondestructive evaluations, underwater acoustics and many other fields.[1–3] Piezoelectric materials are key components in ultrasonic transducers whose electromechanical properties determine the upper limit of transducer performance. Although high-end medical imaging transducers are now made of PMN-PT single crystals, low- and medium-end ultrasonic transducers are still using piezoelectric ceramics due to the advantage of simple preparation process, low production cost, and good electromechanical properties. In recent years, piezoelectric ceramics research has made substantial advance with piezoelectric properties getting close to that of PMN-PT single crystals.[4–7] However, the electromechanical coupling factor $k_{33}$ of piezoceramics is still far inferior to that of PMN-PT single crystals, which limits the performance of ceramic-based transducers.

Texture engineering is an effective method for improving the electromechanical properties of materials.[8] Contrast to conventional ceramic preparation methods, texture engineering introduces directionally oriented template seed crystals into the ceramic, which guide the grain growth process to produce oriented grains in the ceramic. Currently, researchers have obtained some piezoelectric ceramics with excellent electromechanical properties through texture engineering, which demonstrate high potential to replace expensive single crystals currently used in high-end ultrasonic transducers.[9–12] Yang *et al*. investigated textured $Pb(In_{1/2}Nb_{1/2})$-$O_3$–$Pb(Sc_{1/2}Nb_{1/2})O_3$–$PbTiO_3$(PIN-PSN-PT) ceramics. After texturing, the piezoelectric coefficient $d_{33}$ of the ceramic can reach 1090 pC/N, while the electromechanical coupling factor $k_{33}$ can reach 90%.[13] Yan *et al*. prepared $Eu^{3+}$-doped $Pb(Mg_{1/3}Nb_{2/3})$ $O_3$–$PbTiO_3$ (PMN-PT) textured ceramics with piezoelectric coefficient up to 1950 pC/N.[14] These piezoelectric properties are far better than that of traditional PZT-5H piezoelectric ceramic.

$Pb(Ni_{1/3}Nb_{2/3})O_3$–$PbZrO_3$–$PbTiO_3$(PNN-PZT) ceramics have received extensive attention in recent years due to their excellent electromechanical properties.[15–17] Compared to other ceramic systems, PNN-PZT ceramics have the advantages of simple sintering process and high reproducibility. In addition, texture engineering often requires calcined powders with small particle size to ensure the driving force during the texture sintering process. PNN-PZT ceramics can solve this problem by lowering the calcination temperature. The impure phase brought about by lowering the calcination temperature will not affect the final ceramic to achieve pure perovskite phase, while impure phase is often a troubling issue for many other ferroelectric ceramic systems.

[§,‖]Corresponding authors.

[#]These authors contributed equally to this work.

In this work, we selected 0.36PNN–0.24PZ–0.40PT composition with similar Curie temperature to that of commercial PZT-5H ceramic as the matrix and prepared 0.36PNN–0.24PZ–0.40PT textured ceramics by texture engineering using <001> oriented $BaTiO_3$(BT) as the template. Ultrasonic transducers were prepared using PNN-PZT ceramics, PNN-PZT textured ceramics and commercial PZT-5H ceramic. The insertion loss and bandwidth of these ultrasonic transducers were measured and compared. Finally, the corresponding relationship between the performance of piezoelectric ceramics and the performance of transducer is summarized.

## 2. Experimental Procedure

### 2.1. *Preparation of calcined PNN-PZT powder*

PNN-PZT ceramic matrix powder was prepared by solid-state reaction method. NiO (from Aladdin, 99%), $Nb_2O_5$ (from Aladdin, 99.99%), $ZrO_2$ (from D&B, 99.9%), $TiO_2$ (from Aladdin, 99.9%), and PbO (from Aladdin, 99.9%) were used as raw materials for the reaction. Each raw material was weighed according to the stoichiometric ratio, while PbO is in excess of 1 mol% and NiO is in excess of 0.5 mol%. The raw materials were placed in a nylon jar and alcohol was added as solvent to ball mill for 24 h. Afterward, the mixture was dried rapidly in an oven at 110°C. The dried powder was placed in a covered alumina crucible, put into a muffle furnace, ramped up to 700°C at 5°C/min and held for 2 h, then naturally cooled down to room temperature to obtain the calcined powders, which does not need to be in pure perovskite phase. The calcined powders were ball-milled again for 24 h.

### 2.2. *Preparation of PNN-PZT ceramics*

For nontextured ceramics, the powders were mixed well with 7 wt.% PVA solution and pressed into 13 mm diameter discs under a pressure of 200 MPa. The mass of PVB solution is 10% of that of ceramic powder. These discs were placed in a resistance wire furnace and ramped up to 600°C at the rate of 1°C/min, held for 2 h to evaporate PVA binders, then cooled down naturally to room temperature. Based on our experience, the optimal sintering conditions of nontextured ceramics are as follows: the temperature was first raised to 1050°C at the heating rate of 5°C/min and held for 1 h, then raised to 1250°C at the heating rate of 2°C/min and held for 2.5 h, then naturally cooled down to room temperature.

### 2.3. *Preparation of <001>BT*

<001>BT templates were prepared by a three-step process. In the first step, $TiO_2$, $Bi_2O_3$ were used as reactants and NaCl, KCl as molten salts, flakes of $Bi_4Ti_3O_{12}$ were obtained by holding the mixture at 1100°C for 2 h. In the second step, $Bi_4Ti_3O_{12}$, $TiO_2$ and $BaCO_3$ were used as raw materials, and $BaCl_2$–$2H_2O$ and KCl were used as molten salts, flakes of $BaBi_4Ti_4O_{15}$ were obtained by holding them at 1080°C for 2 h. In the third step, $BaBi_4Ti_4O_{15}$ and $BaCO_3$ were used as reactants, and NaCl, KCl was used as molten salt, BT template flakes were obtained by holding the mixture at 980°C for 6 h.

### 2.4. *PNN-PZT textured ceramics*

The tape casting slurry consists of BT templates, calcined powders, solvent, plasticizer and binder. The solvent chosen here is a mixture of alcohol and xylene with a mass ratio of 1:1, the plasticizer is di-n-octyl phthalate, and the binder is polyvinyl butyral. After ball milling the mixture for 12 h, BT templates were added and ball milled for 0.5 h to obtain the casting slurry. During the tape casting process, the scraper height was set to 0.25 mm and the film strips moving speed was set to 1 mm/s. Dried film strips were cut into small discs of 13 mm in diameter, laminated and pressed into 1 mm thin sheets under 150 MPa pressure. In order to effectively eliminate the organic matter in the sample, the temperature was increased to 600°C at the rate of 0.3°C/min, held for 2 h, then naturally cooled down to room temperature. Compared to nontextured ceramics, textured ceramics used lower sintering temperature and longer holding time. We found the optimal sintering conditions for textured ceramics were as follows: first holding the temperature at 750°C for 1 h, then holding at 1000°C for 6 h.

### 2.5. *Characterization of microstructure and electromechanical properties*

The phase structure of these samples was characterized using powder X-ray diffraction (XRD, D/max 2400, Rigaku Corporation, Tokyo, Japan). The microscopic morphology of these samples was observed using scanning electron microscopy (SEM, HELIOS NanoLab 600i, FEI Corporation, OR, USA). Prior to electrical properties testing, all samples were poled at 50°C under a DC electric field of 30 kV/cm for 10 min. The piezoelectric coefficient $d_{33}$ of the material was measured using a quasistatic $d_{33}$ meter (ZJ-4A, Institute of Acoustics, Chinese Academy of Sciences, Beijing, China). The change of capacitance with temperature at different frequencies was measured using an LCR meter (Agilent E4980A, Agilent Technologies, CA, USA) with a temperature chamber, and the change of dielectric constant with temperature was calculated based on the capacitance measurements. The ferroelectric hysteresis loops (*P*–*E*) of these materials were measured using a ferroelectric test system (TF Analyzer 2000E, aixACCT, Germany).

### 2.6. *Performance characterization of transducers*

Pulse-echo response measurements were used to characterize the performance of ultrasonic transducers. A pulse/receiver

(5073PR, Olympus, Japan) was used to send an electrical pulse signal, where the reputation rate is set to 500 Hz, electrical impulse energy is 2 $\mu$J, and the damping factor is 50 Ω. Pulse-echo response was received and displayed on a digital phosphor oscilloscope (DPO4104, Tektronix, USA). The frequency spectrum was obtained by fast Fourier transform of the pulse-echo waveform and the center frequency and bandwidth of the transducer are obtained from the frequency spectrum. A function/arbitrary waveform generator (DG1022, Rigol, China) was used to measure the insertion loss. The waveform generator emitted a 30-cycle sine wave with a voltage amplitude of $V_i$ at the center frequency of the transducer. The voltage value $V_O$ of the received echo response is obtained and measured using an oscilloscope. The insertion loss is calculated according to the following equation:

$$IL = 20\log\left(\frac{V_O}{V_i}\right). \quad (1)$$

## 3. Results and Discussion

The XRD pattern samples are shown in Fig. 1(a), all samples show pure perovskite phase. For nontextured PNN-PZT ceramics, the presence of tiny splits near the peak at 45° indicates that multiphase coexists in these ceramics. In contrast, the textured ceramics exhibit distinct (100) and (200) peaks, while other peaks nearly vanished. The peak splitting near 45° is more pronounced after texture engineering, which implies an increase of the tetragonal phase content in the ceramic. It is found that the Lotgering factor $F_{001}$ of textured ceramics can reach 97%, indicating an excellent alignment of grains along $[001]_c$. Figures 1(b) and 1(d) show the surface and fracture surface morphologies of the textured ceramic, respectively. The grain size of textured ceramic is around 20 $\mu$m, and BT templates are about 10 $\mu$m long and 1 $\mu$m thick embedded inside the grains. In addition, a small number of very small size grains can be observed at the grain boundaries, which are nonoriented grains not involved in the texture process. Figure 1(c) shows the surface morphology of PNN-PZT ceramics, it can be seen that the grain size is in the range of 2–7 $\mu$m, which is much smaller than the grain size of textured ceramics.

Figure 2(a) shows the $P-E$ hysteresis loops of textured and nontextured PNN-PZT ceramics. The textured and nontextured samples exhibit similar coercive field $E_c$, both around 6.4 kV/cm. Compared with nontextured ceramics, textured samples exhibit lower remnant polarization $P_r$ and maximum polarization $P_{max}$. This phenomenon is due to the increase of <001> oriented grains within the ceramic after texturing.[18] Figure 2(b) compares the temperature dependent dielectric behavior of samples at 1 kHz before and after texturing process. Unlike some reported results, textured and nontextured ceramics exhibit similar Curie temperatures $T_c$, both are at

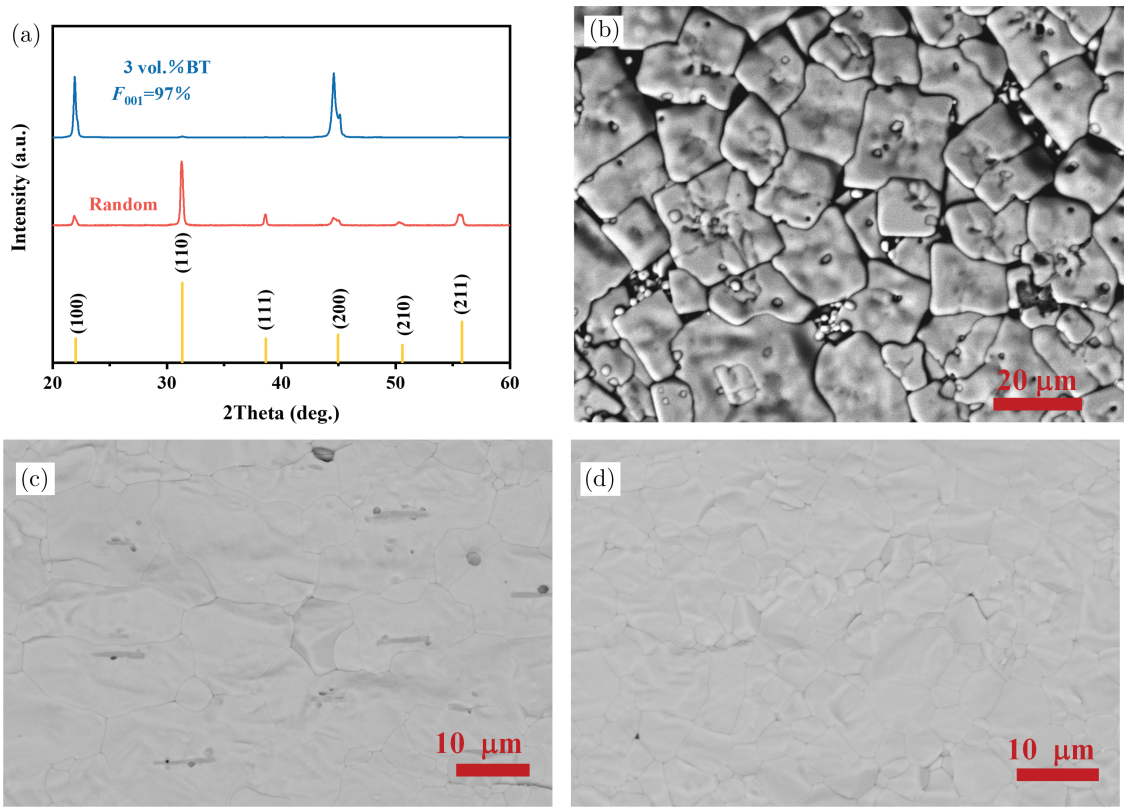


Fig. 1. (a) XRD patterns of nontextured ceramic and textured ceramic, (b) Surface morphology of textured ceramics, (c) Fracture surface morphology of textured ceramics, and (d) Surface morphology of nontextured ceramics.

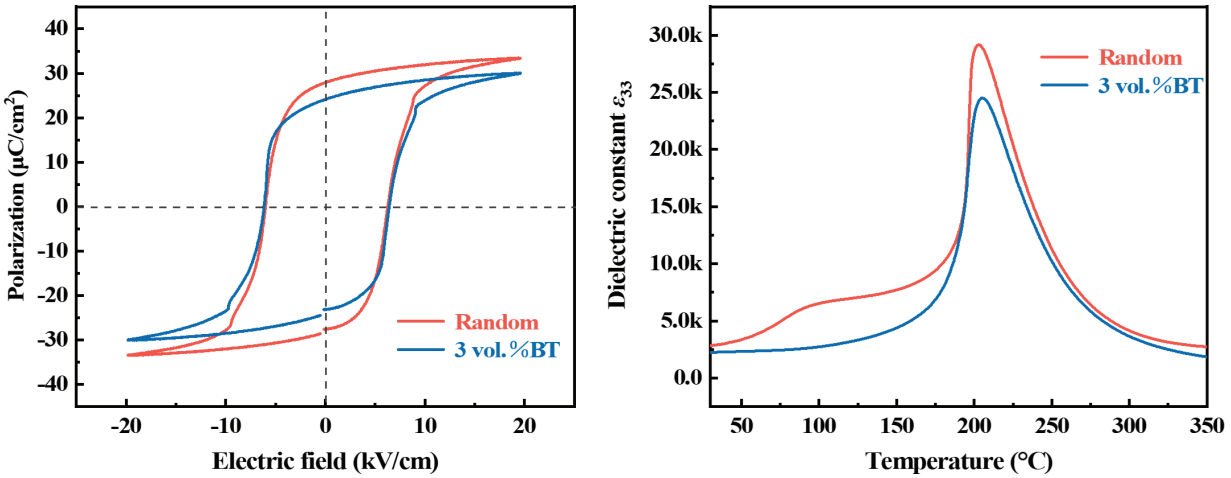


(a) (b)

Fig. 2. (a) *P–E* hysteresis loops of nontextured ceramic and textured ceramic. (b) Dielectric permittivity as a function of temperature for nontextured ceramic and textured ceramic.

203°C. It can be seen that the permittivity $\varepsilon_{33}$ at room temperature and the maximum permittivity $\varepsilon_{max}$ of the textured ceramics are reduced, which is due to the introduction of BT templates with lower dielectric properties.[19] Furthermore, for nontextured ceramics, there is a distinct dielectric peak at 95°C, which represents the rhombohedral(R)-tetragonal(T)-phase transition temperature. However, this distinct peak disappears in textured ceramics and the curve is very flat below 100°C.

The depolarization temperature of ceramics is an important parameter of piezoelectric ceramics. To determine this temperature, we annealed the samples at different temperatures and the holding time was set to 10 min. After cooling back to room temperature, the change in the piezoelectric coefficient was measured, and the test results are shown in Fig. 3(a). For nontextured ceramics, when the annealing temperature exceeds 120°C, the ceramic piezoelectric coefficient begins to show a significant decrease, and when the annealing temperature is 160°C, the ceramic is completely depolarized. For textured ceramics, a small decrease in the ceramic piezoelectric coefficient occurs when the temperature is higher than 90°C. When the temperature is higher than 120°C, changing trend becomes similar to that of nontextured ceramic. The piezoelectric properties of textured ceramics are more susceptible to annealing temperature than those of nontextured ceramics in the temperature range below from 90°C to 120°C, which may be due to the presence of more internal stresses in textured ceramics.

The electromechanical coupling factor is one of the most important parameters of piezoelectric ceramics, and its

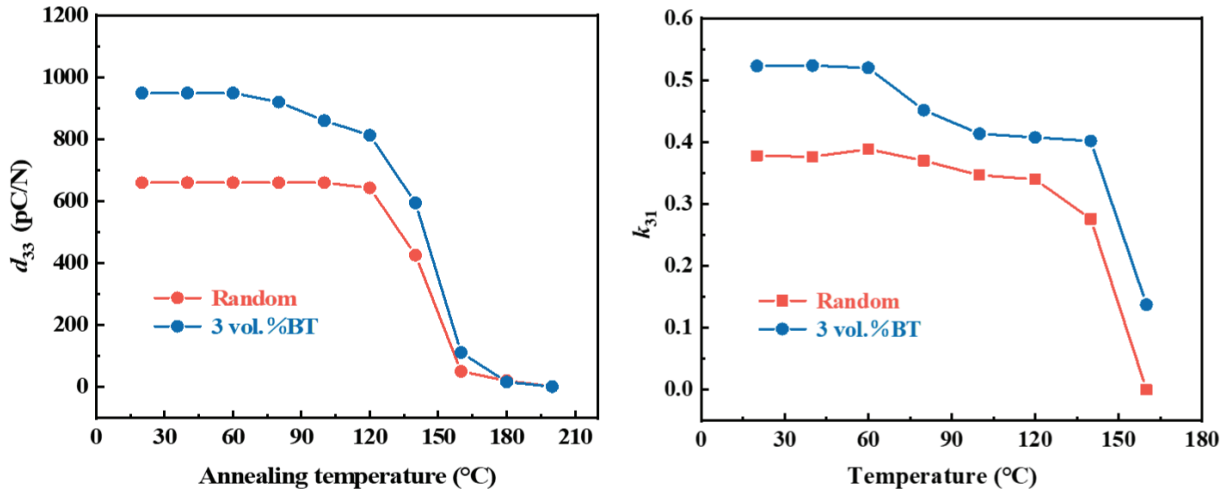


(a) (b)

Fig. 3. (a) The variation of piezoelectric coefficient with annealing temperature. (b) The temperature dependence of electromechanical coupling factor $k_{31}$.

temperature stability is extremely important for device applications. Because the resonance peak corresponding to $k_t$ splits during the warming process leading to significant measurement errors, $k_{31}$ was chosen to measure the electromechanical properties at different temperatures. It is noted that the two types of samples exhibit similar temperature dependence. Figure 3(b) shows the change of $k_{31}$ of samples with temperature. After holding all samples at the corresponding temperature for 10 min, the resonant frequency and the anti-resonant frequency were measured, and the $k_{31}$ was calculated using the following equation:

$$\frac{k_{31}^2}{1-k_{31}^2} = \frac{\pi f_a}{2f_r} \tan \frac{\pi(f_a - f_r)}{2f_r}. \quad (2)$$

It can be seen that $k_{31}$ does not change for all samples when the temperature is below 60°C. When the temperature is higher than 60°C and lower than 140°C, the $k_{31}$ of textured ceramics gradually decreases, but is still higher than that of nontextured ceramics, while the $k_{31}$ of nontextured ceramics is almost a constant. When the temperature is higher than 140°C, the $k_{31}$ of all samples dropped sharply. The comparison of performance parameters of all samples and commercial PZT-5H is given in Table 1. It can be seen that PNN-PZT ceramics have phase transition temperatures with piezoelectric coefficients similar to those of commercial PZT-5H. The permittivity of PNN-PZT ceramics is slightly lower than that of commercial PZT-5H, while PNN-PZT ceramics have a higher electromechanical coupling factor $k_t$ than PZT-5H.

Table 1. Electromechanical properties of PNN-PZT ceramic, textured ceramic and PZT-5H ceramic.

| | $d_{33}$(pC/N) | $T_c$(°C) | $T_{R\text{-}T}$(°C) | $\varepsilon_{33}$ | tan $\delta$ | $k_t$ |
|---|---|---|---|---|---|---|
| PNN-PZT | 680 | 203 | 80~120 | 2832 | 1.6% | 0.51 |
| PNN-PZT-3 vol.%BT | 920 | 203 | — | 2230 | 2.3% | 0.55 |
| PZT-5H | 680 | 191 | 80~120 | 3287 | 1.8% | 0.46 |

PNN-PZT textured ceramics exhibit significantly better electromechanical properties compared to nontextured PNN-PZT ceramics and PZT-5H ceramics.

In order to see the influence of material properties on the transducer performance, piezoelectric transducers were prepared using these three types of piezoelectric ceramics. As shown in Fig. 4(a), the transducer is composed of a matching layer, a piezoelectric ceramic disk, backing layer, wires and housing. The prepared transducers are shown in Fig. 4(b). The metal housing material is aluminum, and the wire material is copper. The acoustic parameters of the matching layer, piezoelectric material and backing layer are given in Table 2. All transducers have the same thickness of matching layer, backing layer and piezoelectric ceramic, where the matching layer material is made of E-51 epoxy resin mixed with 100 nm alumina at a mass ratio of 1:1, and the backing layer material is made of E-51 epoxy resin mixed with 5 $\mu$m tungsten powders at a mass ratio of 1:8.5.

The pulse-echo waveforms and frequency spectra of the three transducers are given in Fig. 5. The PNN-PZT ceramic and PZT-5H ceramic transducers have similar pulse-echo waveforms and both have a long ring-down tail. In contrast, the textured ceramic transducer has a cleaner pulse-echo waveform, as shown in Fig. 5(c).

The performance parameters of these transducers, including the center frequency, insertion loss and −6 dB bandwidth of the transducers are given in Table 3. The PNN-PZT ceramic transducer has nearly equal insertion loss to that of PZT-5H transducer due to the fact that both have the same piezoelectric coefficient. In contrast, PNN-PZT textured ceramic transducer has significantly higher piezoelectric coefficient and therefore its insertion loss is smaller by more than 3 dB. The −6 dB bandwidth of the transducer depends on the electromechanical coupling factor of the ceramic, the PZT-5H ceramic has the smallest electromechanical coupling factor, so the bandwidth is significantly lower than the other two transducers. It is known that increasing the piezoelectric coefficient

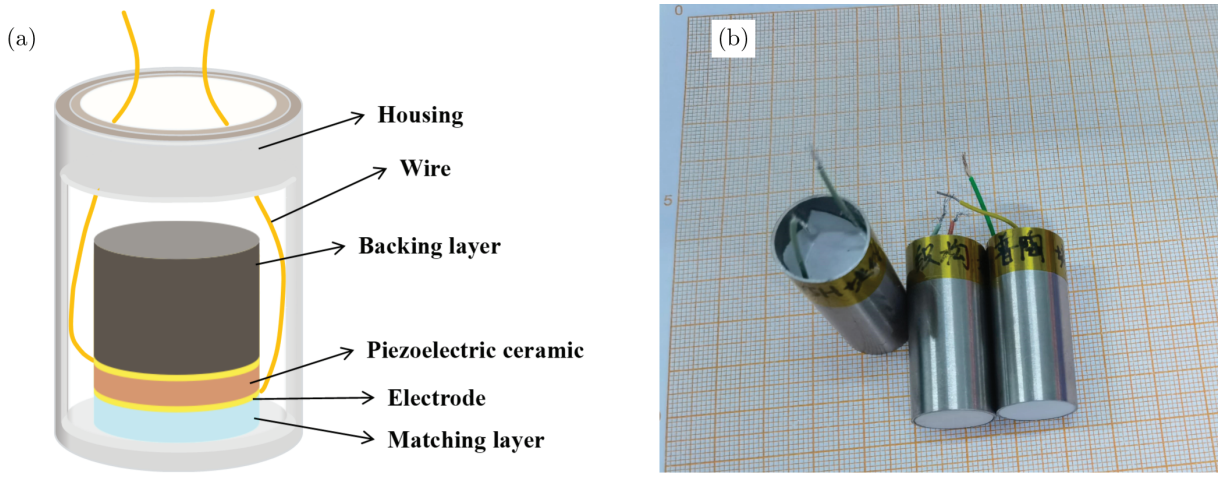


Fig. 4. (a) Structure diagram of transducer. (b) Physical drawing of transducer.

Table 2. Acoustic parameters of the matching layer, piezoelectric material and backing layer.

| | PNN-PZT | PNN-PZT-3 vol.%BT | PZT-5H | Matching layer | Backing layer |
|---|---|---|---|---|---|
| Density $\rho$ (g/cm$^3$) | 7.6 | 7.5 | 7.4 | 1.7 | 7.2 |
| Diameter (mm) | 11.61 | 11.54 | 11 | — | — |
| Longitudinal acoustic velocity $v$ (m/s) | 4010 | 3920 | 4500 | 2810 | 1580 |
| Acoustic impedance $Z$ (MRayls) | 30.5 | 29.4 | 33.3 | 4.9 | 11.4 |
| Thickness $t$ (mm) | 0.75 | 0.75 | 0.75 | 0.23 | 30 |
| Frequency constant $N_t$ (kHz·mm) | 2145 | 1810 | 2250 | — | — |
| Impedance at resonance point (W) | 24.3 | 35.7 | 25.1 | — | — |
| Acoustic attenuation coefficient at 3 MHz $a$ (dB/cm) | — | — | — | 1 | 10 |

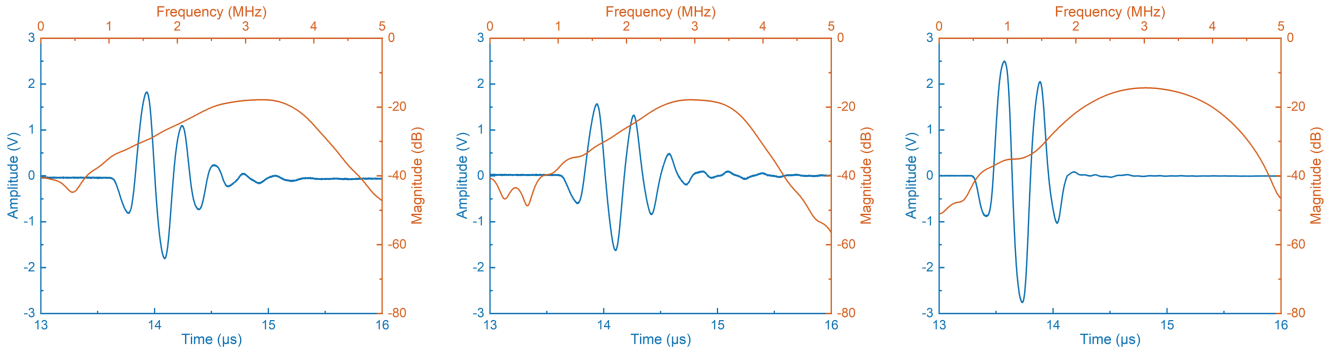


Fig. 5. Pulse-echo waveform and frequency spectrum of the (a) PNN-PZT ceramic transducer, (b) PZT-5H ceramic transducer and (c) PNN-PZT textured ceramic transducer.

Table 3. Performance parameters of the transducer.

| Transducer | Center frequency (MHz) | Insertion loss (dB) | −6 dB bandwidth (%) |
|---|---|---|---|
| PNN-PZT | 3.03 | −17.89 | 59.95% |
| PNN-PZT-3 vol.%BT | 3.05 | −14.43 | 63.65% |
| PZT-5H | 2.95 | −17.90 | 53.11% |

of the piezoelectric ceramic can reduce the insertion loss or increase the sensitivity of the transducer. On the other hand, the electromechanical coupling factor of the ceramic is the determining factor for the bandwidth of the transducer. Therefore, for practical transducer applications, it is important to enhance both the piezoelectric coefficient as well as the electromechanical coupling factor of piezoelectric material.

## 4. Conclusion

In conclusion, PNN-PZT ceramics were modified by texture engineering, which substantially improved its piezoelectric coefficient ($d_{33}$ ~ 920 pC/N) with improved electromechanical coupling factor ($k_t$ ~ 0.55). Single element ultrasonic transducers were made using PNN-PZT ceramic, PNN-PZT textured ceramic and PZT-5H ceramic, and their performance were characterized and compared. The results show that textured PNN-PZT ceramic transducer has much smaller insertion loss or higher sensitivity (more than 3 dB better) due to its larger piezoelectric coefficient. In addition, due to the improved electromechanical coupling factor, the bandwidth of textured PNN-PZT ceramic transducer is also increased. Therefore, texture engineering is an effective method to increase the piezoelectric properties as well as increase the electromechanical coupling factor of piezoelectric ceramics, which are all very important for ultrasonic transducers. It is expected that with further optimization of transducer designs, the textured PNN-PZT ceramics may replace PMN-PT single crystals in high-end medical imaging transducers.

## Acknowledgments

This work was supported by the National Natural Science Foundation of China (Grant No. 51975160).

## References

[1]S. Zhang, F. Li, X. Jiang, J. Kim, J. Luo and X. Geng, Advantages and challenges of relaxor-$PbTiO_3$ ferroelectric crystals for electroacoustic transducers — A review, *Prog. Mater. Sci.* **68**, 1 (2015).

[2]J. W. Hunt, M. Arditi and F. S. Foster, Ultrasound transducers for pulse-echo medical imaging, *IEEE Trans. Biomed. Eng.* **30**, 453 (1983).
[3]J. Jung, W. Lee, W. Kang, E. Shin, J. Ryu and H. Choi, Review of piezoelectric micromachined ultrasonic transducers and their applications, *J. Micromech. Microeng.* **27**, 113001 (2017).
[4]F. Li, D. Lin, Z. Chen, Z. Cheng, J. Wang, C. Li, Z. Xu, Q. Huang, X. Liao, L. Chen, T. R. Shrout and S. Zhang, Ultrahigh piezoelectricity in ferroelectric ceramics by design, *Nat. Mater.* **17**, 349 (2018).
[5]L. Bian, X. Qi, K. Li, J. Fan, Z. Li, E. Sun, B. Yang, S. Dong and W. Cao, High-performance $Pb(Ni_{1/3}Nb_{2/3})O_3$-$PbZrO_3$-$PbTiO_3$ ceramics with the triple point composition, *J. Eur. Ceram. Soc.* **41**, 6983 (2021).
[6]X. Gao, J. Wu, Y. Yu, Z. Chu, H. Shi and S. Dong, Giant piezoelectric coefficients in relaxor piezoelectric ceramic PNN-PZT for vibration energy harvesting, *Adv. Funct. Mater.* **28**, 1706895 (2018).
[7]Q. Guo, F. Li, F. Xia, X. Gao, P. Wang, H. Hao, H. Sun, H. Liu and S. Zhang, High performance Sm-doped $Pb(Mg_{1/3}Nb_{2/3})O_3$-$PbZrO_3$-$PbTiO_3$ based piezoceramics, *ACS Appl. Mater. Interfaces* **11**, 43359 (2019).
[8]A. D. Moriana and S. Zhang, Lead-free textured piezoceramics using tape casting: A review, *J. Materiomics* **4**, 277 (2018).
[9]Y. Yan, Y. Wang and S. Priya, Electromechanical behavior of [001]-textured $Pb(Mg_{1/3}Nb_{2/3})O_3$-$PbTiO_3$ ceramics, *Appl. Phys. Lett.* **100**, 192905 (2012).
[10]Y. Yan, J. Zhou, D. Maurya, Y. Wang and S. Priya, Giant piezoelectric voltage coefficient in grain-oriented modified $PbTiO_3$ material, *Nat. Commun.* **7**, 13089 (2016).
[11]Y. Chang, J. Wu, Z. Liu, E. Sun, L. Liu, Q. Kou, F. Li, B. Yang and W. Cao, Grain-oriented ferroelectric ceramics with single-crystal-like piezoelectric properties and low texture temperature, *ACS Appl. Mater. Interfaces* **12**, 38415 (2020).
[12]L. Liu, B. Yang, S. Yang, Q. Kou, H. Xie, Y. Sun, Y. Chang, S. Zhang and F. Li, Cu-modified $Pb(Mg_{1/3}Nb_{2/3})O_3$-$PbZrO_3$-$PbTiO_3$ textured ceramics with enhanced electromechanical properties and improved thermal stability, *J. Eur. Ceram. Soc.* **42**, 2743 (2022).
[13]S. Yang, J. Li, Y. Liu, M. Wang, L. Qiao, X. Gao, Y. Chang, H. Du, Z. Xu, S. Zhang and F. Li, Textured ferroelectric ceramics with high electromechanical coupling factors over a broad temperature range, *Nat. Commun.* **12**, 1 (2021).
[14]Y. Yan, L. D. Geng, L. Zhu, H. Leng, X. Li, H. Liu, D. Lin, K. Wang, Y. U. Wang and S. Priya, Ultrahigh piezoelectric performance through synergistic compositional and microstructural engineering, *Adv. Sci*. **9**, 2105715 (2022).
[15]J. Du, J. Qiu, K. Zhu and H. Ji, Enhanced piezoelectric properties of $0.55Pb(Ni_{1/3}Nb_{2/3})O_3$-$0.135PbZrO_3$-$0.315PbTiO_3$ ternary ceramics by optimizing sintering temperature, *J. Electroceram.* **32**, 234 (2014).
[16]F. Guo, S. Zhang, W. Long, P. Fang, X. Li and Z. Xi, $SnO_2$ modified PNN-PZT ceramics with ultra-high piezoelectric and dielectric properties, *Ceram. Int.* **48**, 23241 (2022).
[17]H. Wang, F. Zhang, Y. Chen, C. Huang, X. Wang, X. Wu, Y. Chen, Y. Xu, S. Guan, J. Zhu, Q. Chen and J. Xing, Giant piezoelectric coefficient of PNN-PZT-based relaxor piezoelectric ceramics by constructing an R-T MPB, *Ceram. Int.* **47**, 12284 (2021).
[18]L. Bian, Q. Kou, L. Liu, H. Zheng, N. Wang, X. Qi, B. Yang and W. Cao, Enhancing temperature stability of 0.42PNN-0.21PZ-0.37PT ceramics through texture engineering, *ACS Appl. Mater. Interfaces* **14**, 3076 (2022).
[19]Y. Chang, J. Wu, B. Yang, H. Xie, S. Yang, Y. Sun, S. Zhang, F. Li and W. Cao, Large, thermally stabilized and fatigue-resistant piezoelectric strain response in textured relaxor-$PbTiO_3$ ferroelectric ceramics, *J. Mater. Chem. C* **9**, 2008 (2021).